catalysts

MDPI

Article

CO and CO_2 Methanation over CeO_2-Supported Cobalt Catalysts

Thuy Ha Nguyen [1], Han Bom Kim [1] and Eun Duck Park [1,2,*]

[1] Department of Energy System Research, Ajou University, 206, World-Cup-Ro, Yeongtong-Gu, Suwon 16499, Korea; ntthuyha@ajou.ac.kr (T.H.N.); madinga@ajou.ac.kr (H.B.K.)
[2] Department of Chemical Engineering, Ajou University, 206, World-Cup-Ro, Yeongtong-Gu, Suwon 16499, Korea
* Correspondence: edpark@ajou.ac.kr; Tel.: +82-31-219-2384; Fax: 82-31-219-1612

Abstract: CO_2 methanation is a promising reaction for utilizing CO_2 using hydrogen generated by renewable energy. In this study, CO and CO_2 methanation were examined over ceria-supported cobalt catalysts with low cobalt contents. The catalysts were prepared using a wet impregnation and co-precipitation method and pretreated at different temperatures. These preparation variables affected the catalytic performance as well as the physicochemical properties. These properties were characterized using various techniques including N_2 physisorption, X-ray diffraction, H_2 chemisorption, temperature-programmed reduction with H_2, and temperature-programmed desorption after CO_2 chemisorption. Among the prepared catalysts, the ceria-supported cobalt catalyst that was prepared using a wet impregnation method calcined in air at 500 °C, and reduced in H_2 at 500 °C, showed the best catalytic performance. It is closely related to the large catalytically active surface area, large surface area, and large number of basic sites. The in situ diffuse reflectance infrared Fourier transform spectroscopy (DRIFTS) study revealed the presence of carbonate, bicarbonate, formate, and CO on metallic cobalt.

Keywords: CO_2 methanation; CO methanation; cobalt; ceria; Co/CeO_2

Citation: Nguyen, T.H.; Kim, H.B.; Park, E.D. CO and CO_2 Methanation over CeO_2-Supported Cobalt Catalysts. *Catalysts* **2022**, *12*, 212. https://doi.org/10.3390/catal12020212

Academic Editor: Anastasia Macario

Received: 28 December 2021
Accepted: 9 February 2022
Published: 11 February 2022

1. Introduction

CO_2 capture, utilization, and storage have become increasingly important in terms of mitigating global climate change caused by escalation in CO_2 atmospheric concentrations since the first industrial revolution. CO_2 utilization can be categorized into physical and chemical methods. The latter is preferred over the former as CO_2 can be converted into other chemicals through chemical transformations [1]. Among the various chemical utilization methods of CO_2, CO_2 hydrogenation has attracted significant attention as it can produce various platform chemicals, including methane, methanol, and formic acid. It can also utilize hydrogen generated from water with a water electrolysis system powered by renewable energy [2–4].

In particular, CO_2 methanation is considered an energy storage alternative to address variability in renewable energy as the produced methane can be transported through a gas grid. Furthermore, CO_2 methanation (Reaction 1) is thermodynamically more feasible than other CO_2 hydrogenation reactions (e.g., reverse water-gas-shift reaction (Reaction 2) and methanol synthesis (Reaction 3)) [5–7].

Reaction 1:

$$CO_2(g) + 4H_2(g) \rightarrow CH_4(g) + 2H_2O(g)\ \Delta G^{o}_{298\ K} = -113.2\ kJ/mol,\ \Delta H^{o}_{298\ K} = -165\ kJ/mol$$

Reaction 2:

$$CO_2(g) + H_2(g) \rightarrow CO(g) + H_2O(g)\ \Delta G^{o}_{298\ K} = 28.6\ kJ/mol,\ \Delta H^{o}_{298\ K} = 41.2\ kJ/mol$$

Reaction 3:

$$CO_2(g) + 3H_2(g) \rightarrow CH_3OH(g) + H_2O(g)\ \Delta G^{o}_{298\ K} = 3.5\ kJ/mol,\ \Delta H^{o}_{298\ K} = -49.5\ kJ/mol$$

Since CO_2 methanation is an exothermic and thermodynamically limited reaction, active catalysts at low temperatures should be developed. To date, some metal catalysts, including Ru [8–11], Ni [12–19], Co [20–26], and Fe [23,27–29] have been reported to be active in this reaction. However, Ni-based catalysts have been more thoroughly investigated due to their high activity and comparatively low cost [3,4]. In addition to the active metal, the nature of the support also affects the catalytic properties, such as the morphology of the active metal, metal dispersion, and reducibility of active metal/metal oxides [1,2,7]. Several metal oxide supports have been reported for CO_2 methanation reactions, such as Al_2O_3 [30–32], CeO_2 [33–35], SiO_2 [36–38], ZrO_2 [39–42], TiO_2 [43–45], La_2O_3 [45–48], Y_2O_3 [31,49], and Sm_2O_3 [50,51]. Among them, CeO_2 is a well-known support due to its redox properties and high surface oxygen vacancies. In particular, two oxidation states of cerium (e.g., Ce^{3+} and Ce^{4+}) are interconvertible between CeO_2 and CeO_{2-x} under oxidized and reduced environments to release oxygen vacancy [52–55]. This is favorable for the dissociation of CO_2 into CO and O species on the catalyst surface in the dissociative CO_2 methanation mechanisms [52–54]. The other representative CO_2 methanation mechanism is the associative one, in which the chemisorbed CO_2 ($CO_{2\ ads}$) and chemisorbed H_2 ($H_{2\ ads}$) species are found on the support surface and the active sites, respectively. In this CO_2 associative reaction mechanism, several intermediates such as carbonate, bicarbonate, and formate are observed [1].

Additionally, catalytic performance is influenced by the catalyst preparation methods, such as precipitation [56], co-precipitation [57], wet impregnation [21,58], and co-wet impregnation [59]. The wet-impregnation method is a well-known traditional method that is simple and economical. However, this generally provides a weaker metal-support interaction than the co-precipitation method [60]. Pretreatment conditions are also key factors in controlling the structural properties of the catalysts [61,62].

In this study, cobalt and ceria were chosen as the active metal and support, respectively. Although cobalt is more expensive than nickel, cobalt is more stable under low-temperature reaction conditions than nickel as using nickel can result in the formation of unstable nickel carbonyl complexes in the presence of CO, especially at low temperatures. The cobalt content was fixed to low enough so that the catalyst price could be comparable with those of typical nickel-based catalysts with high nickel content (higher than 10 wt.%). Two preparation methods, wet impregnation and co-precipitation, were conducted in this study. The effect of pretreatment temperature on the catalytic performance was also investigated.

2. Results and Discussion

2.1. Physicochemical Properties of the Prepared Catalysts

The textural properties of the prepared catalysts were determined using N_2 physisorption. Figure S1 shows the N_2 adsorption and desorption isotherms of each catalyst. The impregnated samples (Co/CeO_2) show a Type IV physisorption isotherm with an H2(a) hysteresis loop. The co-precipitated catalysts ($Co_{0.1}Ce_{0.9}O_x$) exhibited a Type III physisorption isotherm with an H3 hysteresis loop. As listed in Table 1, the Brunauer-Emmett-Teller (BET) surface area of the catalyst decreased, however the average pore diameter of the catalyst increased with increasing calcination temperature, irrespective of the preparation method.

Table 1. Physicochemical properties of ceria-supported cobalt catalysts [a].

Catalysts	BET Surface Area [b] (m^2/g)	Pore Volume [b] (cm^3/g)	Average Pore Diameter [b] (nm)	Cobalt Dispersion [c] (%)	CASA [c] (m^2/g_{cat})	CO_2 Uptake [d] ($\mu mol/g_{cat}$)
$Co_{0.1}Ce_{0.9}O_x$(300)	90	0.23	10.2	4.65	0.74	124
$Co_{0.1}Ce_{0.9}O_x$(500)	72	0.28	18.9	5.98	0.95	146
$Co_{0.1}Ce_{0.9}O_x$(700)	34	0.22	26.3	3.27	0.52	59
Co/CeO_2(300)	130	0.12	3.9	3.87	0.94	196
Co/CeO_2(500)	128	0.14	4.3	4.65	1.13	186
Co/CeO_2(700)	60	0.13	8.6	3.72	0.90	122

[a] All catalysts were calcined in air at different temperatures and reduced in H_2 at 500 °C. [b] The data were determined with N_2 physisorption. [c] The data were calculated based on H_2 chemisorption. [d] The data were quantified based on pulsed CO_2 chemisorption.

The cobalt contents of the impregnated and co-precipitated samples were determined to be 5.3 and 3.3 wt.%, respectively. The catalytically active surface area (CASA) of each catalyst was determined by H_2 chemisorption. Interestingly, the CASA and cobalt dispersions show a volcano plot as a function of the calcination temperature, irrespective of the preparation method. $Co_{0.1}Ce_{0.9}O_x$(500) and Co/CeO_2(500) have the largest CASA among the catalysts prepared using the co-precipitation and wet impregnation methods, respectively. The number of surface basic sites was measured using pulsed CO_2 chemisorption. Of the co-precipitated catalysts, the largest number of surface basic sites was obtained for $Co_{0.1}Ce_{0.9}O_x$(500). The number of surface basic sites decreased with increasing calcination temperature for the Co/CeO_2 catalysts prepared using the wet impregnation method.

The bulk crystalline structures of the ceria-supported cobalt catalysts before and after reduction were probed using X-ray diffraction (XRD). Figure S2 reveals that the XRD peaks due to CeO_2 (JCPDS 34-0394) are dominant for the samples before reduction. The crystallite size of CeO_2 for the co-precipitated sample increased from 6.5 to 17.7 nm with increasing calcination temperature from 300 to 700 °C, respectively. Similarly, the crystallite size of CeO_2 for the impregnated samples also increased from 6.7 to 12.1 nm with increasing calcination temperature from 300 to 700 °C, respectively. As a result of the low cobalt content, the XRD peaks due to Co_3O_4 (JCPDS 42-1467) were found only for samples calcined at 700 °C, irrespective of the preparation method.

Temperature-programmed reduction with H_2 (H_2-TPR) was conducted to determine the reducibility of metal oxides in each catalyst. The H_2-TPR peaks can be divided into two regions: low-temperature and high-temperature. The low-temperature H_2-TPR peaks range from 100 to 600 °C. These H_2-TPR peaks are related to the reduction in cobalt oxides with different sizes and interactions with ceria. Generally, smaller metal oxides with weak interactions with a support can be reduced more easily at lower temperatures. Conversely, metal oxides with a strong interaction with a support can be reduced at high temperatures, even though the size of metal oxides is small. In the case of Co_3O_4, a two-step reduction process from Co_3O_4 to cobalt through CoO is well known [63]. The high-temperature H_2-TPR peak above 600 °C was ascribed to the reduction in surface ceria. As shown in Figure 1, the Co/CeO_2 catalysts prepared using the wet impregnation method have H_2-TPR peaks at lower temperatures than the $Co_{0.1}Ce_{0.9}O_x$ catalysts prepared using a co-precipitation method. This indicates that the co-precipitation method can provide a stronger interaction between cobalt oxides and ceria than the wet impregnation method. It is noteworthy that the H_2-TPR peak position moves toward a high temperature with increasing calcination temperature, irrespective of the preparation method. This reveals that a stronger interaction between cobalt oxides and ceria can be achieved at higher calcination temperatures.

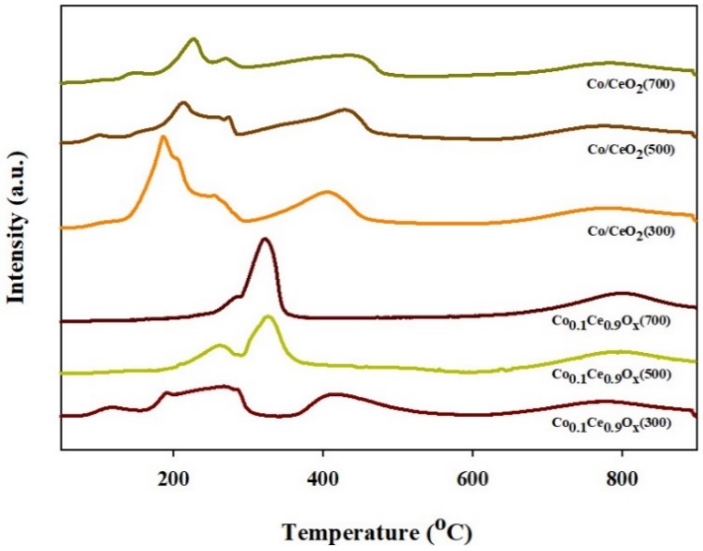

Figure 1. H_2-TPR patterns of ceria-supported cobalt catalysts calcined in air at different temperatures.

Temperature-programmed desorption after CO_2 chemisorption (CO_2-TPD) was performed to probe the surface basicity of each catalyst. As shown in Figure 2, there are two desorption peaks. The first occurs at temperatures less than 200 °C, and the second occurs at temperatures ranging from 200–600 °C. The low-temperature CO_2-TPD peaks originate from weakly adsorbed CO_2 on the catalyst surface, while the high-temperature CO_2-TPD peaks indicate the strong adsorption of CO_2 onto the catalyst surface. The CO_2-TPD peak observed at higher temperatures implies stronger chemisorption of CO_2 onto the catalyst surface. The $Co_{0.1}Ce_{0.9}O_x$(300) catalyst presents no low-temperature CO_2-TPD peak, although it has two CO_2-TPD peaks at high temperatures. However, all other catalysts exhibited low-temperature and high-temperature CO_2-TPD peaks. These two CO_2-TPD peaks were quantified, and the amounts of desorbed CO_2 for each catalyst are listed in Table S1. The amount of strongly chemisorbed CO_2 decreased with increasing calcination temperature for the co-precipitated catalyst ($Co_{0.1}Ce_{0.9}O_x$). The smallest amount of strongly chemisorbed CO_2 was obtained for the $Co_{0.1}Ce_{0.9}O_x$(700) catalyst. Similarly, the amount of strongly chemisorbed CO_2 decreased with increasing calcination temperature for the impregnated catalysts (Co/CeO_2). The smallest amount of strongly chemisorbed CO_2 was obtained for the Co/CeO_2(700) catalyst.

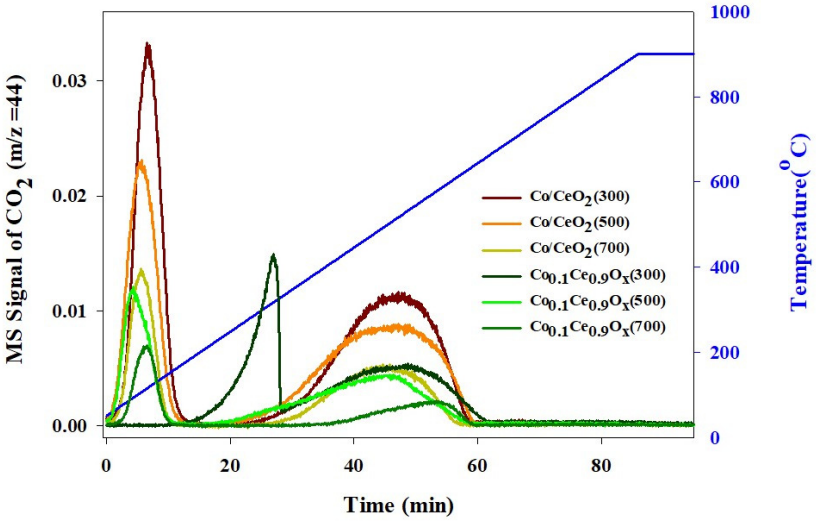

Figure 2. CO_2-TPD profiles of ceria-supported cobalt catalysts calcined in air at different temperatures and reduced in H_2 at 500 °C.

2.2. CO Methanation

The catalytic activity for CO methanation was evaluated using ceria-supported Co catalysts. As shown in Figure 3, the $Co/CeO_2(500)$ catalyst exhibited the highest CO conversion at low temperatures of the tested catalysts, whereas $Co_{0.1}Ce_{0.9}O_x(700)$ showed the lowest CO conversion even at high temperatures. As shown in Figures S3 and S4, CH_4 is the main product, and a small amount of C_2H_6 is also detected as a byproduct. Separately, the specific reaction rate of CO methanation was also obtained under a kinetically controlled regime. The specific reaction rate decreased in the following order: $Co/CeO_2(500)$ > $Co/CeO_2(300)$~$Co_{0.1}Ce_{0.9}O_x(300)$ > $Co_{0.1}Ce_{0.9}O_x(500)$~$Co/CeO_2(700)$ > $Co_{0.1}Ce_{0.9}O_x(700)$. This ranking order in the specific reaction rate is closely related to that of CASA (Table 1) for Co/CeO_2 catalysts. This implies that the catalytic activity for CO methanation is directly related to the catalytically active surface area.

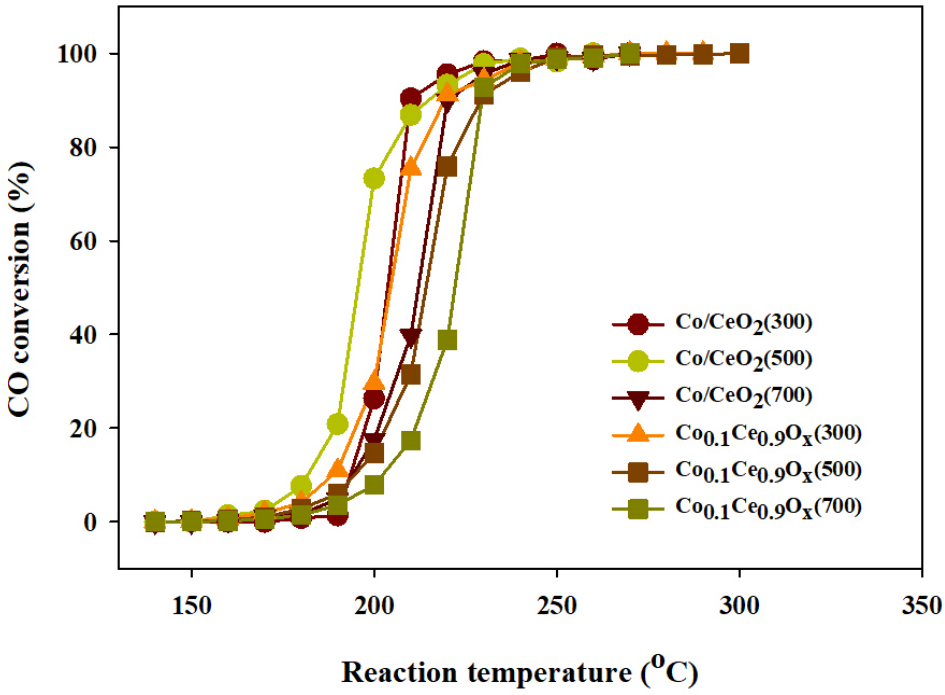

Figure 3. Catalytic activity for CO methanation over ceria-supported cobalt catalysts. All catalysts were reduced in H_2 at 500 °C. The feed gas is composed of 1 mol% CO, 49 mol% He, and 50 mol% H_2, and the total flow rate is 100 mL/min.

The apparent activation energy (E_a) for CO methanation, calculated from the Arrhenius plot in Figure S5 over $Co/CeO_2(300)$, $Co/CeO_2(500)$, $Co/CeO_2(700)$, $Co_{0.1}Ce_{0.9}O_x(300)$, $Co_{0.1}Ce_{0.9}O_x(500)$, and $Co_{0.1}Ce_{0.9}O_x(700)$ were 128, 107, 129, 128, 146, and 162 kJ/mol, respectively. It is worth mentioning that the lowest apparent activation energy is obtained for the catalyst with the largest CASA among Co/CeO_2 catalysts. The fact that the co-precipitated $Co_{0.1}Ce_{0.9}O_x$ catalysts have higher apparent activation energies than the impregnated Co/CeO_2 catalysts seems to be related to the H_2-TPR results that the co-precipitation method can provide a stronger interaction between cobalt oxides and ceria than the wet impregnation method. Castillo et al. [64] reported that the CO consumption turnover rate was significantly lower for smaller cobalt nanoparticles during CO methanation over Co/SiO_2 catalysts with different cobalt particle sizes ranging from 4 to 33 nm. The apparent activation energy was lower for smaller cobalt nanoparticles. The apparent activation energies for CO methanation over 10 wt.% Ni/CeO_2 and 58 wt.% $Ni\text{-}CeO_2$ were reported to be 115 and 133 kJ/mol, respectively [65].

2.3. CO_2 Methanation

The catalytic activity for CO_2 methanation was examined using ceria-supported cobalt catalysts. As shown in Figure 4, the tested catalysts are classified into three groups based on their catalytic activity for CO_2 methanation. The most active catalyst groups include $Co/CeO_2(300)$, $Co/CeO_2(500)$, and $Co/CeO_2(700)$. The $Co_{0.1}Ce_{0.9}O_x(300)$ catalyst was inferior to the most active catalyst group in this reaction. However, it was better than the least active catalyst groups ($Co_{0.1}Ce_{0.9}O_x(500)$ and $Co_{0.1}Ce_{0.9}O_x(700)$). Unlike CO methanation, the catalytic activity for CO_2 methanation over ceria-supported cobalt catalysts tested in this study was not directly correlated with that of CASA (Table 1). In addition to CASA, the amount of moderate basic sites has been reported to be an additional factor affecting the catalytic activity for CO_2 methanation [66]. It is worth mentioning that the least active catalyst ($Co_{0.1}Ce_{0.9}O_x(700)$) had the lowest CO_2 uptake among the prepared catalysts. Methane was produced as the main product, and CO was also detected as a byproduct due to the reversed water-gas-shift side reaction (Figures S6 and S7). The apparent E_a for CO_2 methanation calculated from the Arrhenius plot in Figure S8 over $Co/CeO_2(300)$, $Co/CeO_2(500)$, $Co/CeO_2(700)$, $Co_{0.1}Ce_{0.9}O_x(300)$, $Co_{0.1}Ce_{0.9}O_x(500)$, and $Co_{0.1}Ce_{0.9}O_x(700)$ were 81, 77, 86, 81, 84, and 86 kJ/mol, respectively. Interestingly, all catalysts have similar apparent activation energies. The reported activation energies for CO_2 methanation over nickel-based catalysts range between 55 and 106 kJ/mol [47,67]. The apparent activation energies for CO_2 methanation over 58 wt.% Ni-CeO_2 were reported to be 95 kJ/mol [65]. Xu et al. [41] reported a higher activation energy for CO_2 methanation over Ni/ZrO_2 (99.7 kJ/mol) than over $Ni/Y_{0.1}Zr_{0.9}O_x$ (84.2 kJ/mol). Furthermore, the activation energy of the $Co/Ce_{0.8}Zr_{0.2}O$ catalyst was reported to be less than that of $Ni/Ce_{0.8}Zr_{0.2}O$ catalysts [68].

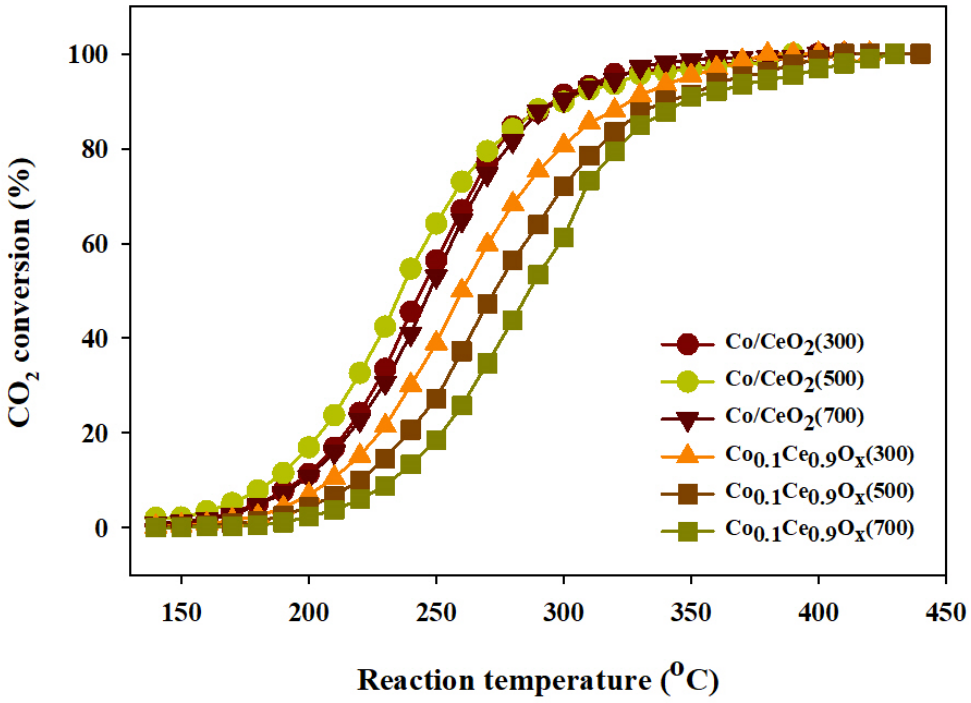

Figure 4. Catalytic activity for CO_2 methanation over ceria-supported cobalt catalysts. All catalysts were reduced in H_2 at 500 °C. The feed gas is composed of 1 mol% CO_2, 49 mol% He, and 50 mol% H_2, and the total flow rate is 100 mL/min.

2.4. In Situ DRIFTS Study

To probe the surface species during CO_2 adsorption and methanation, in situ diffuse reflectance infrared Fourier transform spectroscopy (DRIFTS) study was conducted over the most active catalysts selected from co-precipitated and impregnated catalysts (e.g.,

$Co_{0.1}Ce_{0.9}O_x$(300) and Co/CeO_2(500)). The molecularly absorbed CO_2 was observed at ν = 2400-2200 cm^{-1} [69]. CO_2 adsorption was initially performed at 40 °C (Figure 5). The typical IR peaks observed in this study are listed in Table 2. Bicarbonate and carbonate species were detected during CO_2 adsorption. For the bicarbonate intermediate species, asymmetric and symmetric stretching of OCO (ν_{asy}(OCO) and ν_s(OCO)) were observed at ν = 1602 and 1408 cm^{-1} over $Co_{0.1}Ce_{0.9}O_x$(300). The same bands were observed at ν = 1654 and 1434 cm^{-1} over Co/CeO_2(500). In addition, COH stretching for bicarbonate species (HCO_3^-) clearly appeared at ν = 1217 cm^{-1} over $Co_{0.1}Ce_{0.9}O_x$(300), while it was not observed for Co/CeO_2(500). For the carbonate species, monodentate and bidentate were confirmed over Co/CeO_2(500) at ν_{asy}(OCO) = 1475 and 1577 cm^{-1} and ν_s(OCO) = 1380, 1331, and 1265 cm^{-1}, while the symmetric OCO peak centered at ν = 1293 cm^{-1} was detected for $Co_{0.1}Ce_{0.9}O_x$(300). During CO_2 adsorption at 300 °C (Figures S9 and S10), the bicarbonate and carbonate species also occurred at the same position as at 40 °C. However, the noticeable difference during CO_2 adsorption at low and high temperatures is the weak and broad peaks of adsorbed CO* species on the metallic cobalt at ν = 2184, 2142, 2045, and 2119 cm^{-1} over $Co_{0.1}Ce_{0.9}O_x$(300) and Co/CeO_2(500). This implies that the C=O double bond in the CO_2 molecule can be broken down to generate CO* intermediates at high temperatures.

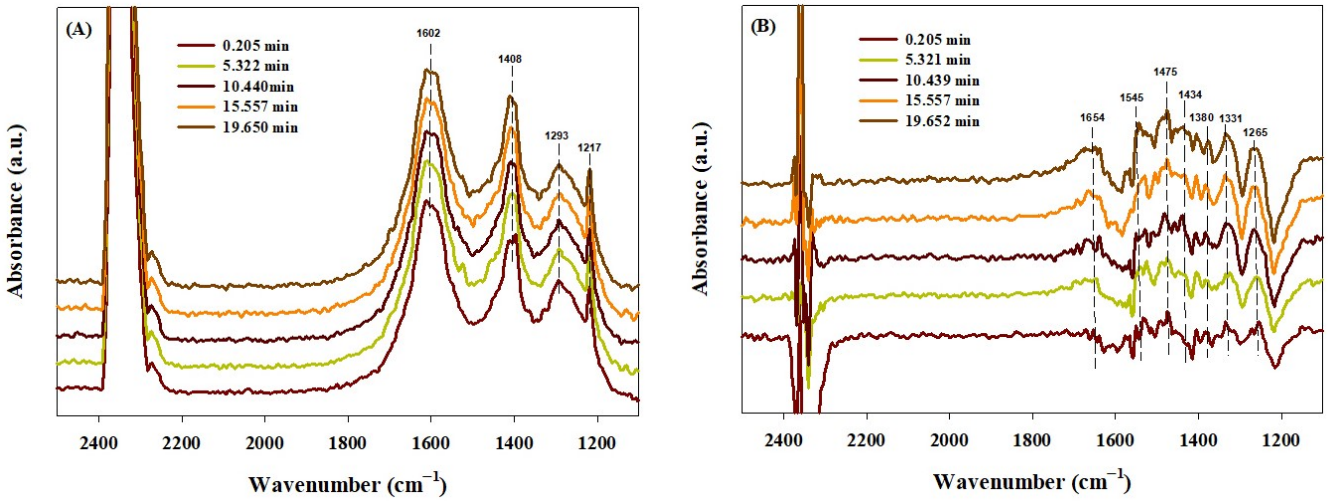

Figure 5. In situ DRIFTS spectra after adsorption of CO_2 on $Co_{0.1}Ce_{0.9}O_x$(300) (**A**) and Co/CeO_2(500) (**B**) at 40 °C. The feed gas is composed of 10 mol% CO_2 and 90 mol% He.

The in situ DRIFTS study was also conducted during CO_2 methanation with increasing reaction temperature. Figures 6 and 7 show the IR spectra of $Co_{0.1}Ce_{0.9}O_x$(300) and Co/CeO_2(500), respectively. The observed IR bands are summarized in Table 2. The sharp IR peak at ν = 1216 cm^{-1}, which can be ascribed to COH stretching at temperatures below 300 °C, is responsible for the bicarbonate species observed over both $Co_{0.1}Ce_{0.9}O_x$(300) and Co/CeO_2(500). Furthermore, carbonate species were found in the monodentate and bidentate forms, whereas the OCO and CO vibrations were obtained in the range of ν = 1575 and ν = 1075 cm^{-1}. In particular, the specific formate species, which are common intermediates during CO_2 hydrogenation, were also found in the stretching of CH and OCO at the high-frequency adsorption band. The vibrations at ν = 2944–2713 cm^{-1} are ascribed to CH stretching. The weak vibration of adsorbed CO* species on metallic cobalt was also detected at ν = 2115 and 2075 cm^{-1} over $Co_{0.1}Ce_{0.9}O_x$(300), while Co^{n+}-CO bridged species were only observed at ν = 2115 cm^{-1} over Co/CeO_2(500). In addition, methane adsorbed on the catalyst surface was detected at ν = 1305 and 3014 cm^{-1}. Based on the IR study, it can be proposed that the CO_2 associative pathway is the main route as a result of the predominant appearance of bicarbonate, carbonate, and formate intermediates. However,

the CO_2 dissociative route cannot be excluded to produce methane over ceria-supported cobalt catalysts.

Table 2. FT-IR peaks during CO_2 adsorption and hydrogenation over $Co_{0.1}Ce_{0.9}O_x$(300) and Co/CeO_2(500).

Vibrational Mode Assignments	IR Peak Position (cm^{-1})							References
	$Co_{0.1}Ce_{0.9}O_x$(300)			Ce/CeO_2(500)			Literature	
	Adsorption		Hydrogenation	Adsorption		Hydrogenation		
	40 °C	300 °C		40 °C	300 °C			
Absorbed CO* species on metallic cobalt		2184 2142 2045	2115 2075		2119	2115	2181, 2168, 2118, 2084, 2048	[70,71]
Absorbed CO_2							2200–2400	[69]
Bicarbonate (HCO_3^-)								
ν(OH)						3636, 3667	3600–3627, 3620	[33,72–74]
ν_{asy}(OCO)	1602			1654			1655, 1652, 1650	
ν_s(OCO)	1408			1434			1440, 1424, 1435	
ν(COH)	1217	1217	1216			1216	1225, 1220, 1228	
Carbonate (CO_3^-)							1550 and 1380	
Monodentate								
ν_{asy}(OCO)						1452	1446–1590	
ν_s(OCO)	1450			1475	1457	1349, 1396	1380–1395	[33,69,74]
ν(CO)	1385		1394	1380	1354	1075	1040	
Bidentate				1545				
ν_{asy}(OCO)			1575	1265	1577		1535–1670	
ν_s(OCO)	1293	1288	1286	1331	1279	1284	1243–1355	
Formate								
ν(CH)			2713, 2849		2848	2838, 2719	2756–2866, 2905	[69,72,73]
ν(OCO)		2850	2944		1523	2940	1540, 1510, 1450	
Methane			3014			1305, 3014	1305 and 3015	[73]

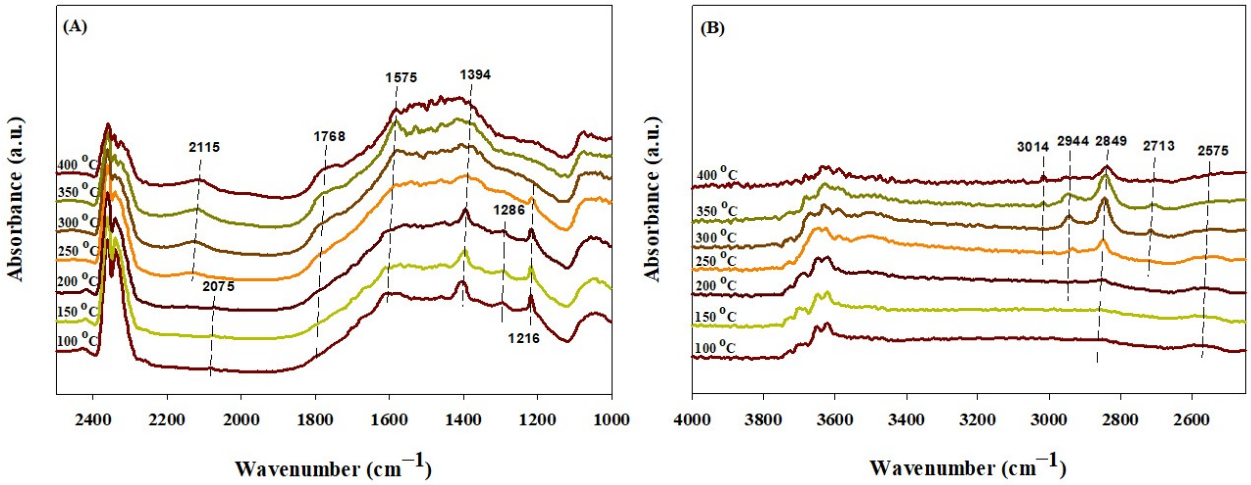

Figure 6. In situ DRIFTS spectra during CO_2 methanation at temperatures of 100-450 °C over the $Co_{0.1}Ce_{0.9}O_x$(300) catalyst in the range of 2500–1000 cm^{-1} (**A**) and 2500-4000 cm^{-1} (**B**). The feed is composed of 1 mol% CO_2, 49 mol% He, and 50 mol% H_2.

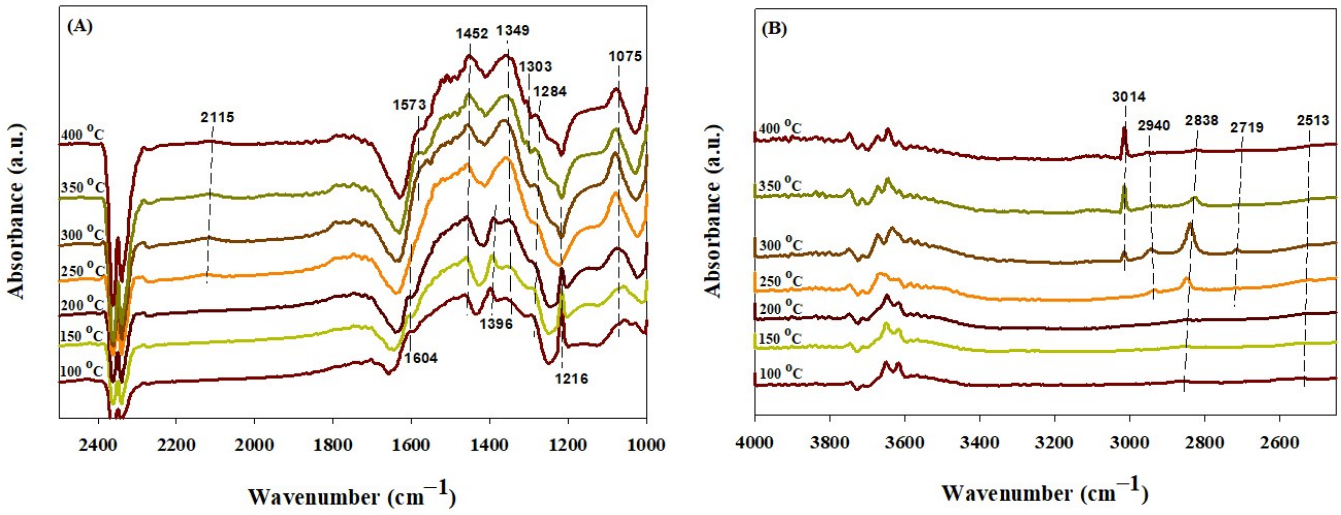

Figure 7. In situ DRIFTS spectra during CO_2 methanation at temperatures of 100–450 °C over the Co/CeO_2(500) catalyst in the range of 2500–1000 cm^{-1} (**A**) and 2500–4000 cm^{-1} (**B**). The feed is composed of 1 mol% CO_2, 49 mol% He, and 50 mol% H_2.

3. Experimental Sections

3.1. Materials

All chemicals, including cobalt (II) nitrate hexahydrate (Junsei Chemical Co. Ltd., Tokyo, Japan), cerium (III) nitrate hexahydrate (Junsei Chemical Co. Ltd., Tokyo, Japan), and ceria (Rodia, S_{BET} = 250 m^2/g), were reagent grade and used as received.

3.2. Preparation of the Catalysts

$Co_{0.1}Ce_{0.9}O_x$ catalysts were prepared using the co-precipitation method. The calculated amount of each precursor was dissolved in distilled (DI) water to achieve 0.1 M total metal precursor solution. The pH was then increased by adding 0.5 M NH_4OH aqueous solution dropwise to reach a final pH of nine with vigorous stirring. The slurry was aged at room temperature for 12 h, filtered, and washed several times with DI water. The recovered solid cake was dried at 110 °C overnight under vacuum conditions. The dried sample was further calcined in air at different temperatures and finally reduced in H_2 at 500 °C.

For comparison, the Co/CeO_2 catalysts were prepared using a wet impregnation method. Cobalt precursor (1.30 g) was dissolved in 50.0 mL DI water in a round flask. Ceria (5.00 g) was added to the cobalt precursor solution. This slurry was mixed for 6 h at 60 °C in a rotary evaporator (BUCHI Labortechnik AG, Flawil, Switzerland), and then the excess water was evaporated while maintaining low pressure. The recovered powder was dried at 110 °C overnight under vacuum conditions. The dried sample was further calcined in air at different temperatures and finally reduced in H_2 at 500 °C.

The calcination temperature was included in the sample name to differentiate each catalyst calcined at different temperatures. For example, $Co_{0.1}Ce_{0.9}O_x$(300) and Co/CeO_2(300) are catalysts prepared by co-precipitation and wet impregnation, respectively. These catalysts were calcined in air at 300 °C.

3.3. Catalyst Characterizations

N_2 physisorption was performed at −196 °C on a Micromeritics ASAP 2020 (Micromeritics Ltd.), surface area and pore size analyzer after degassing at 200 °C under vacuum for 6 h. The specific surface area and pore size distribution were determined using the BET and Barret-Joyner-Halenda desorption methods, respectively.

XRD patterns were measured using a Rigaku D/Max instrument with a Cu K_α source. The crystallite size of ceria was determined using the Scherrer Formula (1):

$$d = \frac{K\lambda}{\beta \cos(\theta)} \quad (1)$$

where d is the average particle size (nm), K is the dimensionless shape factor (0.9), λ is the wavelength of the X-ray radiation (0.15406 nm), β is the full width at half maximum (FWHM) of a peak in rad, and θ is the Bragg angle.

The temperature-programmed reduction with H_2 (H_2-TPR) was conducted using a Micromeritics 2920 Autochem instrument. A sample of 100 mg was loaded in a quartz tube, and the temperature was increased from room temperature (RT) to 900 °C at a heating rate of 10 °C/min under a flow of 10 mol% H_2/Ar.

The H_2-chemisorption was performed using a Micromeritics ASAP 2020 instrument (Micromeritics Ltd.), to determine the metal dispersion and CASA. A sample of 200 mg was placed in a quartz tube, reduced in H_2 at 500 °C for 1 h, cooled down to room temperature, and typical H_2-chemisorption was conducted.

Pulsed CO_2 chemisorption and temperature-programmed desorption after CO_2 chemisorption (CO_2-TPD) were conducted to measure the amount of basic sites and adsorption strength of CO_2 in each sample, respectively. They were performed using a Micromeritics 2920 Autochem instrument. A sample of 100 mg was loaded into a quartz tube, reduced under 10 mol% H_2/Ar flow at 500 °C for 1 h, cooled to room temperature, and received pulsed injection of CO_2. After saturation, CO_2 desorption was conducted using a He steam flow rate of 30 mL/min. The mass ion signals recorded at m/e = 44, m/e = 18, and m/e = 16 were monitored to detect desorbed CO_2, H_2O, and CH_4, respectively.

The metal content in each sample was determined by inductively coupled plasma-optical emission spectroscopy (ICP-OES) using a Thermo Scientific iCAP 6500 instrument.

The evolution of surface species during CO_2 adsorption and CO_2 hydrogenation was probed with in situ DRIFTS on a NICOLET 6700 (Thermal Scientific, Waltham, MA, USA) spectrometer with a ZnSe window at a resolution of 3.857 cm^{-1}. The sample was initially reduced in situ in the DRIFTS cell at 500 °C for 1 h under a H_2 flow rate of 20 mL/min and then cooled to the desired temperature. The cell was purged and stabilized with He flow for 20 min. The background was then collected under a He flow. The CO_2 adsorptions at 40 and 300 °C were separately performed under a flow of 10% CO_2/He, and the spectra were recorded simultaneously. In addition, CO_2 hydrogenation was examined at different temperatures under the same operating conditions mentioned above, and the spectra were collected after 15 min.

3.4. Catalytic Performance

The catalyst (100 mg) was placed in a fixed-bed reactor (internal diameter = 3 mm and length = 345 mm) and reduced under H_2 flow at a flow rate of 30 mL/min for 1 h. The reactor was then cooled to the desired temperature, and the catalyst was placed in contact with a feed composed of 1 mol% CO (or CO_2), 49 mol% He, and 50 mol% H_2 at a flow rate of 100 mL/min. A mass flow rate controller (MFC) (Brooks Instrument) was used to control the flow rate of each gas.

The kinetic experiment was conducted separately using 80 mg of the catalyst and 200 mg of α-alumina powder as a diluent. The CO (or CO_2) conversion was controlled to be less than 20%, and the E_a was calculated using the Arrhenius Equation (2):

$$k = A\exp\left(-\frac{E_a}{RT}\right) \quad (2)$$

where k is the reaction rate constant, A is the frequency factor, E_a is the apparent activation energy, R is the gas constant, and T is the temperature.

The effluent gas was separated using a packed column filled with carbonate for thermal conductive detector (TCD) and a capillary Poralot Q column for the flame ionization detector (FID) in a gas chromatograph (YL Instrument 6100GC). The CO (or CO_2) conver-

sion (X_{CO} or X_{CO_2}, %) and the product yields, including CH_4 and CO (Y_{CH_4} and Y_{CO}, %) were determined according to the carbon balance as follows:

$$X_{CO} = \frac{C_{CO\ input} - C_{CO\ output}}{C_{CO\ input}} \times 100\% \quad (3)$$

$$X_{CO_2} = \frac{C_{CO_2\ input} - C_{CO_2\ output}}{C_{CO_2\ input}} \times 100\% \quad (4)$$

$$Y_{CH_4} = \frac{C_{CH_4\ output}}{C_{CO\ input} + C_{CO_2\ input}} \times 100\% \quad (5)$$

$$Y_{CO} = \frac{C_{CO\ output}}{C_{CO_2\ input}} \times 100\% \quad (6)$$

The input and output concentrations of each gas (i) are denoted as $C_{i\ input}$ and $C_{i\ output}$, respectively.

4. Conclusions

The catalytic activity for CO and CO_2 methanation was dependent on the preparation method for ceria-supported cobalt catalysts with low cobalt contents. Stronger interactions between cobalt oxides and ceria were observed for the co-precipitated catalysts than for wet-impregnated interactions. A moderate calcination temperature is plausible for achieving a high CASA. The total number of basic sites decreased significantly with an increasing calcination temperature of 500 to 700 °C for the co-precipitated and impregnated catalysts. CO methanation activity appears to be closely related to CASA, and the CASA and the number of strong basic sites affect the catalytic activity for CO_2 methanation. According to the in situ DRIFTS results, CO_2 methanation proceeds mainly through the CO_2 associative pathway, in which carbonate, bicarbonate, and formate intermediates are detected. Additionally, the CO_2 dissociative route worked simultaneously as we also observed the adsorbed CO species on the metallic cobalt surface sites.

Supplementary Materials: The following supporting information can be downloaded at: https://www.mdpi.com/article/10.3390/catal12020212/s1, Figure S1: Nitrogen adsorption and desorption isotherms (A,B) and pore size distribution (C) of ceria-supported cobalt catalysts calcined in air at different temperatures. Figure S2: XRD patterns of ceria-supported cobalt catalysts calcined in air at different temperatures (A) and after reduction in H_2 at 500 °C (B). Figure S3: Carbon selectivities for CH_4 and C_2H_6 for CO methanation over ceria-supported cobalt catalysts. Figure S4: Product yields for CO methanation over ceria-supported cobalt catalysts. Figure S5: Arrhenius plot for CO methanation over ceria-supported cobalt catalysts. Figure S6: Carbon selectivities for CH_4 and CO for CO_2 methanation over ceria-supported cobalt catalysts. Figure S7: Product yields for CO_2 methanation over ceria-supported cobalt catalysts. Figure S8: Arrhenius plot for CO_2 methanation over ceria-supported cobalt catalysts. Figure S9. In situ DRIFTS spectra after adsorption of CO_2 on the $Co_{0.1}Ce_{0.9}O_x$(300) catalyst at 300 °C. The feed was composed of 33 mol% CO_2 and 67 mol% He. Figure S10. In situ DRIFTS spectra after adsorption of CO_2 on the Co/CeO_2(500) catalyst at 300 °C. The feed was composed of 10 mol% CO_2 and 90 mol% He. Table S1: Quantitative analysis of the CO_2-TPD data.

Author Contributions: Experimental investigation and data analysis, T.H.N.; formal analysis, H.B.K.; writing—original draft preparation, T.H.N.; writing—review and editing, supervision, project administration, and funding acquisition, E.D.P. All authors have read and agreed to the published version of the manuscript.

Funding: This work was supported by the C1 Gas Refinery Program through the National Research Foundation of Korea (NRF) funded by the Ministry of Science and ICT (2015M3D3A1A01064899).

Conflicts of Interest: The authors declare no conflict of interest.

References

1. Nguyen, T.T.H.; Park, E.D. A mini-review on power-to-methane catalysts. *J. Energy Eng.* **2021**, *30*, 10–25.
2. Sreedhar, I.; Varun, Y.; Singh, S.A.; Venugopal, A.; Reddy, B.M. Developmental trends in CO_2 methanation using various catalysts. *Catal. Sci. Technol.* **2019**, *9*, 4478–4504. [CrossRef]
3. Younas, M.; Loong Kong, L.; Bashir, M.J.K.; Nadeem, H.; Shehzad, A.; Sethupathi, S. Recent advancements, fundamental challenges, and opportunities in catalytic methanation of CO_2. *Energy Fuels* **2016**, *30*, 8815–8831. [CrossRef]
4. Li, W.; Wang, H.; Jiang, X.; Zhu, J.; Liu, Z.; Guo, X.; Song, C. A short review of recent advances in CO_2 hydrogenation to hydrocarbons over heterogeneous catalysts. *RSC Adv.* **2018**, *8*, 7651–7669. [CrossRef]
5. Ashok, J.; Pati, S.; Hongmanorom, P.; Tianxi, Z.; Junmei, C.; Kawi, S. A review of recent catalyst advances in CO_2 methanation processes. *Catal. Today* **2020**, *356*, 471–489. [CrossRef]
6. Bailera, M.; Lisbona, P.; Romeo, L.M.; Espatolero, S. Power to gas projects review: Lab, pilot and demo plants for storing renewable energy and CO_2. *Renew. Sustain. Energy Rev.* **2017**, *69*, 292–312. [CrossRef]
7. Gao, J.; Liu, Q.; Gu, F.; Liu, B.; Zhong, Z.; Su, F. Recent advances in methanation catalysts for the production of synthetic natural gas. *RSC Adv.* **2015**, *5*, 22759–22776. [CrossRef]
8. Garbarino, G.; Bellotti, D.; Riani, P.; Magistri, L.; Busca, G. Methanation of carbon dioxide on Ru/Al_2O_3 and Ni/Al_2O_3 catalysts at atmospheric pressure: Catalysts activation, behaviour and stability. *Int. J. Hydrog. Energy* **2015**, *40*, 9171–9182. [CrossRef]
9. Kim, A.; Sanchez, C.; Haye, B.; Boissière, C.; Sassoye, C.; Debecker, D.P. Mesoporous TiO_2 support materials for Ru-based CO_2 methanation catalysts. *ACS Appl. Nano Mater.* **2019**, *2*, 3220–3230. [CrossRef]
10. Chen, S.; Abdel-Mageed, A.M.; Dyballa, M.; Parlinska-Wojtan, M.; Bansmann, J.; Pollastri, S.; Olivi, L.; Aquilanti, G.; Behm, R.J. Raising the COx methanation activity of a Ru/gamma-Al_2O_3 catalyst by activated modification of metal-support interactions. *Angew. Chem. Int. Ed. Eng.* **2020**, *59*, 22763–22770. [CrossRef]
11. Quindimil, A.; de la Torre, U.; Pereda-Ayo, B.; Davó-Quiñonero, A.; Bailón-García, E.; Lozano-Castelló, D.; González-Marcos, J.A.; Bueno-López, A.; González-Velasco, J.R. Effect of metal loading on the CO_2 methanation: A comparison between alumina supported Ni and Ru catalysts. *Catal. Today* **2020**, *356*, 419–432. [CrossRef]
12. Tan, J.; Wang, J.; Zhang, Z.; Ma, Z.; Wang, L.; Liu, Y. Highly dispersed and stable Ni nanoparticles confined by MgO on ZrO_2 for CO_2 methanation. *Appl. Surf. Sci.* **2019**, *481*, 1538–1548. [CrossRef]
13. Bacariza, M.C.; Amjad, S.; Teixeira, P.; Lopes, J.M.; Henriques, C. Boosting Ni Dispersion on zeolite-supported catalysts for CO_2 methanation: The influence of the impregnation solvent. *Energy Fuels* **2020**, *34*, 14656–14666. [CrossRef]
14. Guilera, J.; del Valle, J.; Alarcón, A.; Díaz, J.A.; Andreu, T. Metal-oxide promoted Ni/Al_2O_3 as CO_2 methanation micro-size catalysts. *J. CO_2 Util.* **2019**, *30*, 11–17. [CrossRef]
15. Song, F.; Zhong, Q.; Yu, Y.; Shi, M.; Wu, Y.; Hu, J.; Song, Y. Obtaining well-dispersed Ni/Al_2O_3 catalyst for CO_2 methanation with a microwave-assisted method. *Int. J. Hydrog. Energy* **2017**, *42*, 4174–4183. [CrossRef]
16. Daroughegi, R.; Meshkani, F.; Rezaei, M. Enhanced activity of CO_2 methanation over mesoporous nanocrystalline Ni–Al_2O_3 catalysts prepared by ultrasound-assisted co-precipitation method. *Int. J. Hydrog. Energy* **2017**, *42*, 15115–15125. [CrossRef]
17. Kesavan, J.K.; Luisetto, I.; Tuti, S.; Meneghini, C.; Iucci, G.; Battocchio, C.; Mobilio, S.; Casciardi, S.; Sisto, R. Nickel supported on YSZ: The effect of Ni particle size on the catalytic activity for CO_2 methanation. *J. CO_2 Util.* **2018**, *23*, 200–211. [CrossRef]
18. Vogt, C.; Groeneveld, E.; Kamsma, G.; Nachtegaal, M.; Lu, L.; Kiely, C.J.; Berben, P.H.; Meirer, F.; Weckhuysen, B.M. Unravelling structure sensitivity in CO_2 hydrogenation over nickel. *Nat. Catal.* **2018**, *1*, 127–134. [CrossRef]
19. Danaci, S.; Protasova, L.; Lefevere, J.; Bedel, L.; Guilet, R.; Marty, P. Efficient CO_2 methanation over Ni/Al_2O_3 coated structured catalysts. *Catal. Today* **2016**, *273*, 234–243. [CrossRef]
20. Zhou, G.; Wu, T.; Xie, H.; Zheng, X. Effects of structure on the carbon dioxide methanation performance of Co-based catalysts. *Int. J. Hydrog. Energy* **2013**, *38*, 10012–10018. [CrossRef]
21. Li, W.; Liu, Y.; Mu, M.; Ding, F.; Liu, Z.; Guo, X.; Song, C. Organic acid-assisted preparation of highly dispersed Co/ZrO_2 catalysts with superior activity for CO_2 methanation. *Appl. Catal. B Environ.* **2019**, *254*, 531–540. [CrossRef]
22. Razzaq, R.; Li, C.; Usman, M.; Suzuki, K.; Zhang, S. A highly active and stable Co_4N/γ-Al_2O_3 catalyst for CO and CO_2 methanation to produce synthetic natural gas (SNG). *Chem. Eng. J.* **2015**, *262*, 1090–1098. [CrossRef]
23. Yu, W.-Z.; Fu, X.-P.; Xu, K.; Ling, C.; Wang, W.-W.; Jia, C.-J. CO_2 methanation catalyzed by a Fe-Co/Al_2O_3 catalyst. *J. Environ. Chem. Eng.* **2021**, *9*, 105594. [CrossRef]
24. Li, W.; Nie, X.; Jiang, X.; Zhang, A.; Ding, F.; Liu, M.; Liu, Z.; Guo, X.; Song, C. ZrO_2 support imparts superior activity and stability of Co catalysts for CO_2 methanation. *Appl. Catal. B Environ.* **2018**, *220*, 397–408. [CrossRef]
25. Li, W.; Zhang, G.; Jiang, X.; Liu, Y.; Zhu, J.; Ding, F.; Liu, Z.; Guo, X.; Song, C. CO_2 hydrogenation on unpromoted and m-promoted Co/TiO_2 catalysts (M = Zr, K, Cs): Effects of crystal phase of supports and metal-support interaction on tuning product distribution. *ACS Catal.* **2019**, *9*, 2739–2751. [CrossRef]
26. Le, T.A.; Kim, M.S.; Lee, S.H.; Park, E.D. CO and CO_2 methanation over supported cobalt catalysts. *Top. Catal.* **2017**, *60*, 714–720. [CrossRef]
27. Satthawong, R.; Koizumi, N.; Song, C.; Prasassarakich, P. Comparative study on CO_2 hydrogenation to higher hydrocarbons over Fe-based bimetallic catalysts. *Top. Catal.* **2013**, *57*, 588–594. [CrossRef]
28. Serrer, M.-A.; Gaur, A.; Jelic, J.; Weber, S.; Fritsch, C.; Clark, A.H.; Saraçi, E.; Studt, F.; Grunwaldt, J.-D. Structural dynamics in Ni–Fe catalysts during CO_2 methanation—Role of iron oxide clusters. *Catal. Sci. Technol.* **2020**, *10*, 7542–7554. [CrossRef]

29. Pastor-Pérez, L.; Shah, M.; le Saché, E.; Ramirez Reina, T. Improving Fe/Al_2O_3 catalysts for the reverse water-gas shift reaction: On the effect of cs as activity/selectivity promoter. *Catalysts* **2018**, *8*, 608. [CrossRef]
30. Rahmani, S.; Rezaei, M.; Meshkani, F. Preparation of highly active nickel catalysts supported on mesoporous nanocrystalline γ-Al_2O_3 for CO_2 methanation. *J. Ind. Eng. Chem.* **2014**, *20*, 1346–1352. [CrossRef]
31. Italiano, C.; Llorca, J.; Pino, L.; Ferraro, M.; Antonucci, V.; Vita, A. CO and CO_2 methanation over Ni catalysts supported on CeO_2, Al_2O_3 and Y_2O_3 oxides. *Appl. Catal. B Environ.* **2020**, *264*, 118494. [CrossRef]
32. Visconti, C.G.; Lietti, L.; Tronconi, E.; Forzatti, P.; Zennaro, R.; Finocchio, E. Fischer–Tropsch synthesis on a Co/Al_2O_3 catalyst with CO_2 containing syngas. *Appl. Catal. A Gen.* **2009**, *355*, 61–68. [CrossRef]
33. Vile, G.; Colussi, S.; Krumeich, F.; Trovarelli, A.; Perez-Ramirez, J. Opposite face sensitivity of $CeO_{(2)}$ in hydrogenation and oxidation catalysis. *Angew. Chem. Int. Ed. Eng.* **2014**, *53*, 12069–12072. [CrossRef] [PubMed]
34. Tada, S.; Shimizu, T.; Kameyama, H.; Haneda, T.; Kikuchi, R. Ni/CeO_2 catalysts with high CO_2 methanation activity and high CH_4 selectivity at low temperatures. *Int. J. Hydrog. Energy* **2012**, *37*, 5527–5531. [CrossRef]
35. Zhou, G.; Liu, H.; Cui, K.; Xie, H.; Jiao, Z.; Zhang, G.; Xiong, K.; Zheng, X. Methanation of carbon dioxide over Ni/CeO_2 catalysts: Effects of support CeO_2 structure. *Int. J. Hydrog. Energy* **2017**, *42*, 16108–16117. [CrossRef]
36. Dias, Y.R.; Perez-Lopez, O.W. Carbon dioxide methanation over Ni-Cu/SiO_2 catalysts. *Energy Convers. Manag.* **2020**, *203*, 112214. [CrossRef]
37. Ye, R.-P.; Gong, W.; Sun, Z.; Sheng, Q.; Shi, X.; Wang, T.; Yao, Y.; Razink, J.J.; Lin, L.; Zhou, Z.; et al. Enhanced stability of Ni/SiO_2 catalyst for CO_2 methanation: Derived from nickel phyllosilicate with strong metal-support interactions. *Energy* **2019**, *188*, 116059. [CrossRef]
38. Park, J.-N.; McFarland, E.W. A highly dispersed Pd–Mg/SiO_2 catalyst active for methanation of CO_2. *J. Catal.* **2009**, *266*, 92–97. [CrossRef]
39. Liu, C.; Wang, W.; Xu, Y.; Li, Z.; Wang, B.; Ma, X. Effect of zirconia morphology on sulfur-resistant methanation performance of MoO_3/ZrO_2 catalyst. *Appl. Surf. Sci.* **2018**, *441*, 482–490. [CrossRef]
40. Zhao, K.; Wang, W.; Li, Z. Highly efficient Ni/ZrO_2 catalysts prepared via combustion method for CO_2 methanation. *J. CO_2 Util.* **2016**, *16*, 236–244. [CrossRef]
41. Xu, X.; Tong, Y.; Huang, J.; Zhu, J.; Fang, X.; Xu, J.; Wang, X. Insights into CO_2 methanation mechanism on cubic ZrO_2 supported Ni catalyst via a combination of experiments and DFT calculations. *Fuel* **2021**, *283*, 118867. [CrossRef]
42. Ren, J.; Qin, X.; Yang, J.-Z.; Qin, Z.-F.; Guo, H.-L.; Lin, J.-Y.; Li, Z. Methanation of carbon dioxide over Ni–M/ZrO_2 (M = Fe, Co, Cu) catalysts: Effect of addition of a second metal. *Fuel Process. Technol.* **2015**, *137*, 204–211. [CrossRef]
43. Chai, S.; Men, Y.; Wang, J.; Liu, S.; Song, Q.; An, W.; Kolb, G. Boosting CO_2 methanation activity on Ru/TiO_2 catalysts by exposing (001) facets of anatase TiO_2. *J. CO_2 Util.* **2019**, *33*, 242–252. [CrossRef]
44. Kim, A.; Debecker, D.P.; Devred, F.; Dubois, V.; Sanchez, C.; Sassoye, C. CO_2 methanation on Ru/TiO_2 catalysts: On the effect of mixing anatase and rutile TiO_2 supports. *Appl. Catal. B Environ.* **2018**, *220*, 615–625. [CrossRef]
45. Liu, J.; Li, C.; Wang, F.; He, S.; Chen, H.; Zhao, Y.; Wei, M.; Evans, D.G.; Duan, X. Enhanced low-temperature activity of CO_2 methanation over highly-dispersed Ni/TiO_2 catalyst. *Catal. Sci. Technol.* **2013**, *3*, 2627–2633. [CrossRef]
46. Song, H.; Yang, J.; Zhao, J.; Chou, L. Methanation of carbon dioxide over a highly dispersed Ni/La_2O_3 catalyst. *Chin. J. Catal.* **2010**, *31*, 21–23. [CrossRef]
47. Takami, K.; Takahash, T. Kinetics of the methanation of carbon dioxide over a supported La_2O_3. *Can. J. Eng.* **1988**, *66*, 343–347.
48. Li, S.; Tang, H.; Gong, D.; Ma, Z.; Liu, Y. Loading Ni/La_2O_3 on SiO_2 for CO methanation from syngas. *Catal. Today* **2017**, *297*, 298–307. [CrossRef]
49. Kock, E.M.; Kogler, M.; Bielz, T.; Klotzer, B.; Penner, S. In situ FT-IR spectroscopic study of CO_2 and CO adsorption on Y_2O_3, ZrO_2, and yttria-stabilized ZrO_2. *J. Phy.s Chem. C Nanomater. Interfaces* **2013**, *117*, 17666–17673. [CrossRef]
50. Ayub, N.A.; Bahruji, H.; Mahadi, A.H. Barium promoted Ni/Sm_2O_3 catalysts for enhanced CO_2 methanation. *RSC Adv.* **2021**, *11*, 31807–31816. [CrossRef]
51. Ilsemann, J.; Sonström, A.; Gesing, T.M.; Anwander, R.; Bäumer, M. Highly active Sm_2O_3-Ni xerogel catalysts for CO_2 methanation. *ChemCatChem* **2019**, *11*, 1732–1741. [CrossRef]
52. Bian, Z.; Chan, Y.M.; Yu, Y.; Kawi, S. Morphology dependence of catalytic properties of Ni/CeO_2 for CO_2 methanation: A kinetic and mechanism study. *Catal. Today* **2020**, *347*, 31–38. [CrossRef]
53. Guo, Y.; Mei, S.; Yuan, K.; Wang, D.-J.; Liu, H.-C.; Yan, C.-H.; Zhang, Y.-W. Low-temperature CO_2 methanation over CeO_2-supported Ru single atoms, nanoclusters, and nanoparticles competitively tuned by strong metal–support interactions and H-spillover effect. *ACS Catal.* **2018**, *8*, 6203–6215. [CrossRef]
54. Ye, R.-P.; Li, Q.; Gong, W.; Wang, T.; Razink, J.J.; Lin, L.; Qin, Y.-Y.; Zhou, Z.; Adidharma, H.; Tang, J.; et al. High-performance of nanostructured Ni/CeO_2 catalyst on CO_2 methanation. *Appl. Catal. B Environ.* **2020**, *268*, 118474. [CrossRef]
55. Sakpal, T.; Lefferts, L. Structure-dependent activity of CeO_2 supported Ru catalysts for CO_2 methanation. *J. Catal.* **2018**, *367*, 171–180. [CrossRef]
56. Jiang, M.; Wang, B.; Yao, Y.; Li, Z.; Ma, X.; Qin, S.; Sun, Q. A comparative study of CeO_2-Al_2O_3 support prepared with different methods and its application on MoO_3/CeO_2-Al_2O_3 catalyst for sulfur-resistant methanation. *Appl. Surf. Sci.* **2013**, *285*, 267–277. [CrossRef]

57. Ho, P.H.; de Luna, G.S.; Angelucci, S.; Canciani, A.; Jones, W.; Decarolis, D.; Ospitali, F.; Aguado, E.R.; Rodríguez-Castellón, E.; Fornasari, G.; et al. Understanding structure-activity relationships in highly active La promoted Ni catalysts for CO_2 methanation. *Appl. Catal. B Environ.* **2020**, *278*, 119256. [CrossRef]
58. Liang, C.; Tian, H.; Gao, G.; Zhang, S.; Liu, Q.; Dong, D.; Hu, X. Methanation of CO_2 over alumina supported nickel or cobalt catalysts: Effects of the coordination between metal and support on formation of the reaction intermediates. *Int. J. Hydrog. Energy* **2020**, *45*, 531–543. [CrossRef]
59. Mihet, M.; Lazar, M.D. Methanation of CO_2 on Ni/γ-Al_2O_3: Influence of Pt, Pd or Rh promotion. *Catal. Today* **2018**, *306*, 294–299. [CrossRef]
60. Hongmanorom, P.; Ashok, J.; Zhang, G.; Bian, Z.; Wai, M.H.; Zeng, Y.; Xi, S.; Borgna, A.; Kawi, S. Enhanced performance and selectivity of CO_2 methanation over phyllosilicate structure derived Ni-Mg/SBA-15 catalysts. *Appl. Catal. B Environ.* **2021**, *282*, 19564. [CrossRef]
61. Li, T.; Wang, S.; Gao, D.-N.; Wang, S.-D. Effect of support calcination temperature on the catalytic properties of Ru/$Ce_{0.8}Zr_{0.2}O_2$ for methanation of carbon dioxide. *J. Fuel Chem. Technol.* **2014**, *42*, 1440–1446. [CrossRef]
62. Wu, H.; Zou, M.; Guo, L.; Ma, F.; Mo, W.; Yu, Y.; Mian, I.; Liu, J.; Yin, S.; Tsubaki, N. Effects of calcination temperatures on the structure–activity relationship of Ni–La/Al_2O_3 catalysts for syngas methanation. *RSC Adv.* **2020**, *10*, 4166–4174. [CrossRef]
63. Sexton, B.A.; Hughes, A.E.; Turney, T.W. An XPS and TPR study of the reduction of promoted cobalt-kieselguhr Fischer-Tropsch catalysts. *J. Catal.* **1986**, *97*, 390–406. [CrossRef]
64. Castillo, J.; Arteaga-Pérez, L.E.; Karelovic, A.; Jiménez, R. The consequences of surface heterogeneity of cobalt nanoparticles on the kinetics of CO methanation. *Catal. Sci. Technol.* **2019**, *9*, 6415–6427. [CrossRef]
65. Le, T.A.; Kim, M.S.; Lee, S.H.; Kim, T.W.; Park, E.D. CO and CO_2 methanation over supported Ni catalysts. *Catal. Today* **2017**, *293–294*, 89–96. [CrossRef]
66. Liu, K.; Xu, X.; Xu, J.; Fang, X.; Liu, L.; Wang, X. The distributions of alkaline earth metal oxides and their promotional effects on Ni/CeO_2 for CO_2 methanation. *J. CO_2 Util.* **2020**, *38*, 113–124. [CrossRef]
67. Le, T.A.; Kim, J.; Kang, J.K.; Park, E.D. CO and CO methanation over Ni/Al@Al_2O_3 core–shell catalyst. *Catal. Today* **2020**, *356*, 622–630. [CrossRef]
68. Xu, L.; Cui, Y.; Chen, M.; Wen, X.; Lv, C.; Wu, X.; Wu, C.-E.; Miao, Z.; Hu, X. Screening transition metals (Mn, Fe, Co, and Cu) promoted Ni-based CO_2 methanation bimetal catalysts with advanced low-temperature activities. *Ind. Eng. Chem. Res.* **2021**, *60*, 8056–8072. [CrossRef]
69. Yu, Y.; Mottaghi-Tabar, S.; Iqbal, M.W.; Yu, A.; Simakov, D.S.A. CO_2 methanation over alumina-supported cobalt oxide and carbide synthesized by reverse microemulsion method. *Catal. Today* **2021**, *379*, 250–261. [CrossRef]
70. Hadjiivanov, K.; Ivanova, E.; Dimitrov, L.; Knözinger, H. FTIR spectroscopic study of CO adsorption on Rh–ZSM-5: Detection of Rh+ −CO species. *J. Mol. Struct.* **2003**, *661–662*, 459–463. [CrossRef]
71. Choi, J.G.; Rhee, H.K.; Moon, S.H. IR and TPD study of fresh and carbon-deposited Co/Al_2O_3 catalysts. *Appl. Catal. A Gen.* **1985**, *13*, 269–280. [CrossRef]
72. Watson, C.D.; Martinelli, M.; Cronauer, D.C.; Kropf, A.J.; Jacobs, G. Low temperature water-gas shift: Enhancing stability through optimizing Rb loading on Pt/ZrO_2. *Catalysts* **2021**, *11*, 210. [CrossRef]
73. Das, T.; Deo, G. Synthesis, characterization and in situ DRIFTS during the CO_2 hydrogenation reaction over supported cobalt catalysts. *J. Mol. Catal. A Chem.* **2011**, *350*, 75–82. [CrossRef]
74. Baltrusaitis, J.; Schuttlefield, J.; Zeitler, E.; Grassian, V.H. Carbon dioxide adsorption on oxide nanoparticle surfaces. *Chem. Eng. J.* **2011**, *170*, 471–481. [CrossRef]